Bonding in intermetallics may be deceptive – the case of the new type structure Au2InGa2

Ghasemi, Masoomeh; Lidin, Sven; Johansson, Jonas; Wang, Fei

Published in:
Intermetallics

DOI:
10.1016/j.intermet.2013.10.013

2014

Bonding in intermetallics may be deceptive – the case of the new type structure Au_2InGa_2

Masoomeh Ghasemi[1], Sven Lidin[2], Jonas Johansson[1], Fei Wang[2]

[1] Solid State Physics, Lund University, Box 118, SE-22100 Lund, Sweden

[2] Polymer and Materials Chemistry, Lund University, Box 124, SE-22100 Lund, Sweden

Corresponding author:

Email address: masoomeh.ghasemi@ftf.lth.se
Postal address: Box 118, SE-22100 Lund, Sweden
Phone: 0046-46 222 0586

Email addresses:

sven.lidin@chem.lu.se
jonas.johansson@ftf.lth.se
fei.wang@chem.lu.se

Abstract

We have investigated the crystal and the electronic structure of a new ternary phase, Au_2InGa_2 using powder and single crystal X-Ray Diffraction (XRD) and Stuttgart Tight Binding LMTO-ASA methods, respectively. Complementary methods including Thermo-Gravimetric Differential Thermal Analysis (TG-DTA), Energy Dispersive x-ray Spectroscopy (EDS) and Scanning Electron Microscopy (SEM) were also employed. As a result, the complete structure was determined and the role of homoatomic and heteroatomic bonding is discussed.

Keywords:

A. intermetallics, miscellaneous; A. ternary alloy system, miscellaneous; B. crystallography; E. electronic structure, calculations.

1. Introduction

Vapor-Liquid-Solid (VLS) growth [1] of mixed Ga, In containing III-V compound semiconductors [2] often involves gold as a solvent and hence the thermodynamics of the ternary system Au-In-Ga are interesting for the understanding of optimal growth conditions [3-5]. During a systematic mapping of an isothermal section of the ternary phase diagram at 280 °C, a previously unknown ternary phase, Au_2InGa_2, was identified from Thermo-Gravimetric-Differential Thermal Analysis (TG-DTA), X-Ray powder Diffraction (XRD), x-ray Energy Dispersive Spectroscopy (EDS) and Scanning Electron Microscopy (SEM). According to preliminary results, the new phase occurs at a gold content of roughly 40 at.%. Powder diffraction reveals a hexagonal unit cell a = 4.20473 (16) Å, c = 12.9673 (5) Å and the systematic absences are indicative of space group 194, $P6_3/mmc$.

The single crystal measurements revealed the fact Au_2InGa_2 is an ordered compound in contrast to previously reported similar structures such as $Au_{0.45}Pt_{1.68}Sn_{2.87}$ [6] and $Au_2In_{1.5}Sn_{1.5}$ [7]. Moreover, the electronic structure calculations display a dominance of heteroatomic interactions (Au-Ga and Au-In) rather than homoatomic Au-Au bonds in the Au_2InGa_2 structure.

2. Materials and Methods

2.1 Sample preparation

The samples were prepared using pure metal foils of Au and In (99.999 mass% and 99.999 mass%, respectively) and pure pellets of Ga (99.9999 mass%). The samples were melted at 1100 °C in sealed, evacuated quartz tubes (~10^{-5} mbar). In order to reach equilibrium the samples were

then annealed at 280 °C for about one to three weeks followed by slow cooling down to room temperature.

For single crystal measurements, a further step was also taken. The ingots of the sample with the composition close to the ternary phase were recrystallized for 35 days at 370 °C, slightly below the melting temperature of the ternary phase.

2.2 Analytical methods

The samples were analyzed using Differential Thermal Analysis (DTA), X-Ray Diffraction (XRD), Energy Dispersive x-ray Spectroscopy (EDS) and Scanning Electron Microscopy (SEM).

For DTA measurements (Jupiter F3 449, Netzsch Co.), a small ingot with the mass of about 50 to 100 mg in an alumina crucible was used. The reference was an empty alumina crucible. To prevent oxidation, the furnace was evacuated and flushed with N_2 three times before thermal cycles. A heating and cooling rate of 10 K/min was used. The results were analyzed using the software delivered with the instrument (NETZSCH Proteus- Thermal Analysis- version 5.1.0).

For powder XRD measurements (STOE Stadi P, Cu-Kα radiation, Mythens detector) a piece of alloy was ground to a powder. The powders were then annealed in sealed quartz tubes at 280 °C for about three days. The calibration of the XRD instruments was performed using Si powder. Then, the sample powders were measured with steps of 0.9 of the detector and 100 s exposure time. The coexistence of phases and the lattice parameters were analyzed using JANA 2006 [8].

Single crystal diffraction analysis was also used to characterize the crystal structure of the new ternary phase. A small fragment with clean surfaces was chosen from the crushed ingot, mounted

on a glass fiber with epoxy glue and single crystal X-ray data was measured at ambient conditions on an Agilent Technologies Xcalibur E instrument. The structure was solved using charge flipping as implemented in Superflip [9] and the structure was refined using JANA2006.

To investigate the microstructure of the samples, both optical (Nikon Optiphot) and scanning electron microscopes (JSM-6700F SEM) were employed. The electron microscope was equipped with an EDS analyzer which was used to measure the local chemical compositions of the samples. For these measurements, samples were embedded into a conductive resin and were polished in three steps with diamond suspensions (9 μm and 1 μm, respectively) and finally with SiO_2 colloidal.

2.3 Electronic Structure Calculations

First principle quantum mechanics calculations were performed with the Stuttgart Tight Binding Linear Muffin-Tin Orbital method employing the Atomic Sphere Approximation (TB-LMTO-ASA) [10]. The atomic spheres and empty spheres were generated and scaled to fill the unit cell with a 9.56% overlap by the default settings of the program. The electronic exchange and correlation was treated with the von Barth-Hedin potential [11]. An 8 × 8 × 8 grid was used to sample the first Brillouin zone. We included only the scalar relativistic effect without involving spin-orbit coupling. The basis sets included Au 6*s*, 6*p*, and 5*d*; In 5*s* and 5*p*; and Ga 4*s* and 4*p*. After self-consistent convergences, we calculated the density of states (DOS) and the negative crystal orbital Hamiltonian population (-COHP) [12] curves.

We then repeated the electronic structure calculations with the ABINIT code [13-15] and made a comparison with the LMTO results. The norm-conserving pseudopotentials with the Perdew-

Burke-Ernzerhof generalized gradient approximation [16, 17] were employed. The energy cutoff value of the plane wave basis set is 287.4 eV. A 7 × 7 × 7 Monkhorst-Pack mesh [18] was used for the first Brillouin zone integration. We also adopted the Methfessel and Paxton occupational smearing scheme [19] (smearing energy 0.1 eV) to facilitate the self-consistent convergence.

3. Results and discussion

3.1 Crystal structure

From powder XRD measurements the new ternary compound Au_2InGa_2 was identified. Local chemical analysis by EDS method and microstructural observations also verified the new phase. The lattice parameters of the hexagonal unit cell of Au_2InGa_2 were found to a = 4.20473 (16) Å, c = 12.9673 (5) using powder data. The incongruent melting point of 394 °C was determined using DTA results.

The SEM image of the post-DTA sample with the composition of 44at.%Au-22at.%In-34at.%Ga as well as the DTA thermogram of the same sample are shown in Figure 1. The highest registered temperature on the heating curve is the incongruent melting point of the Au_2InGa_2. A full analysis of the ternary phase diagram will appear elsewhere [20]. The elemental compositions of the coexisting phases are also listed in the figure. It was found that AuIn and AuGa phases are clearly distinguishable even though there is significant solid solubility of Ga in AuIn and of In in AuGa.

Single crystal data revealed more information on the crystal structure of the ternary compound Au_2InGa_2. All data pertinent to the structural solution and refinement are given in table 1.

Au_2InGa_2 is an ordered ternary variant of the relatively rare Pt_2Sn_3-type ($P6_3/mmc$) where Pt occupies a single 4f Wyckoff position while Sn occurs in 2b and 4f. Apart from the archetypical Pt_2Sn_3 [21] this structure type has been reported as a meta-stable binary phase Pt_2Si_3 [22] as well as for the ternary phases $Au_{0.45}Pt_{1.68}Sn_{2.87}$ and $Au_2In_{1.5}Sn_{1.5}$. The ternary phases are reported as highly disordered, $Au_2In_{1.5}Sn_{1.5}$ displaying In and Sn evenly distributed over the two Sn positions of the archetype and three positions are reported as compositionally disordered in $Au_{0.45}Pt_{1.68}Sn_{2.87}$. Conversely, Au_2InGa_2 displays full elemental ordering with In in the 2b position while Au and Ga occupy separate 4f positions. From our investigations of the ternary phase diagram, it is clear that the compound Au_2InGa_2 has a certain phase width, and we checked our single crystal sample for signs of mixing on the Ga and In positions. Refinement of mixed positions indeed improves the fit between model and data, but only marginally (from 0.0360 to 0.0355) and the relative amounts of Ga on the In position and In on the Ga position refines to 6% and 1% repectively. An indication that mixed position may be of some importance in given by the relatively large thermal parameters of these positions that indicate the presence of different species with different site preference, specifically that Ga replacing In on the 2b position may be displaced away from the mirror plane and that In replacing Ga on the 4f position may have a different value of the c parameter than Ga has. Attempts to model this in the refinement where unsuccessful, most probably due to the relatively weak contribution of such disorder to the scattering. While there is some indication in the refinement of mixed positions, the refined amount of mixing is so small that it was deemed prudent to use the simpler, fully ordered model. The structure is basically a mixed close- packing where hexagonal and cubic packing alternate, the unit cell comprising 10 layers in the sequence ABCBABACAB. The atomic decoration colors the layers in a sequence of five layers GaAuInAuGa (Figure 2). Each indium atom is

surrounded by six gold atoms as nearest neighbors in a trigonal prim, each gallium has four gold neighbors and three gallium neighbors forming a capped trigonal prism while gold has eight neighbors, four gallium, three indium and one gold, together forming a slightly distorted cube.

The homoatomic contacts, restricted to the majority components Ga and Au, are suggestive of bonding, Ga forming the puckered 6^3 nets, typically seen in elemental Sb or Bi with Ga-Ga distances of 2.94Å, slightly longer than in elemental Ga while gold forms Au_2 dumbbells with Au-Au distances of 2.89Å, very similar to those in elemental gold.

3.2 Electronic structure

The occurrence of Au-Au dimers and puckered Ga 6^3 nets in Au_2InGa_2 are intriguing. The bonding situation becomes quite clear from the band structure, DOS, and -COHP curves calculated with LMTO shown in Figure 3-a and from the negative integrated COHP (-ICOHP) in Table 2.

The compound is clearly a metal with no indication of any pseudo gap in the vicinity of the Fermi level (E_F). The DOS curves reveal that the *s* and *p* states from Au, Ga, and In spread all over below the E_F, indicating that they are all actively involved in bonding. Most of the Au 5*d* states are concentrated in a large DOS peak ranging between ca. -6 and -4 eV below E_F, corresponding to a set of flat bands. Considering Au-Au interactions, the states in the lower half of the peak (between ca. -6 and -5 eV) are bonding (positive –COHP values) and those in the upper half (between ca. -5 and -4 eV) are antibonding (negative –COHP values). These are all the features of semi-core states. The integrated –ICOHP values up to the E_F (Table 2) clearly

shows that while the total Au-Au interaction is positive, for each bond it is considerably smaller than that of heteroatomic contacts, and given the small number of Au-Au contacts in the in unit cell, the total effect is marginal. Not surprisingly, the Ga-Ga interactions, emanating from Ga-Ga contacts longer than those in the element, are even weaker, although their number give them an impact on par with the stronger but fewer Au-Au bonds. Therefore, Au_2InGa_2 is stabilized mainly by the Au-Ga and Au-In interactions while Au-Au interactions are not playing a significant role.

Meanwhile, there is also a significant amount of 5*d* states spreading out from the large DOS peak, especially between ca. -4 ~ -2 eV. The bands in this energy range are not flat at all, indicating that they are involved in bonding as well. From the –COHP curves, it is evident that these states are antibonding for Au-Au but strongly bonding with respect to Au-Ga and Au-In, demonstrating that these Au-Au 5*d* antibonding states are stabilized by their strong bonding interactions with neighboring Ga and In atoms. Therefore, we can conclude that Au atoms are paired to form dimers in Au_2InGa_2 mainly by the interactions between the Au and the surrounding Ga and In, not by strong Au-Au bonding as we would intuitively expect.

How the Au 5*d* antibonding states are stabilized by Ga and In is shown pictorially in Figure 3-b. This is an isosurface plot of the wave function (the norm, thus no phase) of the second highest occupied band at the Γ point (marked with a circle in Figure 3-a). This plot is calculated with ABINIT, which gives a band structure and a DOS consistent with those from LMTO (see Supporting Information). The major contributor to this wave function can be identified as the Au $5d_{z2}$ orbitals. And the clear nodes between Au atoms (golden) indicate, the σ^* antibonding states dominate the interactions between the neighboring Au $5d_{z2}$ orbitals. Similarly, there are clear nodes between neighboring Ga atoms (blue). By contrast, there is no node between Au atoms

and their neighboring Ga atoms. Instead, the wavefunction shows significant smearing between the Au and Ga atoms, manifesting the bonding interactions.

4. Conclusion

The new compound Au_2InGa_2 demonstrates a number of interesting principles. First and foremost that bonding in intermetallics cannot be analyzed in terms of geometry only. The homoatomic structural fragments Au_2 dumbbells and two-dimensional, infinite, puckered Ga 6^3-nets are strongly suggestive of bonding, but electronic structure analysis instead points to a situation where the cohesion in the phase is dominated by heteroatomic interactions. Further, it is notable that among the phases in the ternary system Au-In-Ga, the Au_2InGa_2 stands out as having a very narrow composition interval, while most of the binary Au-In and Au-Ga phases allow for substantial In/Ga solubility. For the ternary compound, this does suggest quite specific Au-In and Au-Ga interactions despite its pronounced metallic character.

Acknowledgments

We gratefully acknowledge financial support from the Nanometer Structure Consortium at Lund University (nmC@LU), the Swedish Research Council (VR), and the Knut and Alice Wallenberg Foundation (KAW). We also thank Sören Jeppesen for the excellent technical support.

References

[1] R.S. Wagner, W.C. Ellis, Vapor-Liquid-Solid mechanism of single crystal growth, Appl. Phys. Lett., 4 (1964) 89-90.

[2] J. Johansson, K.A. Dick, Recent advances in semiconductor nanowire heterostructures, CrystEngComm, 13 (2011) 7175-7184.

[3] M. Paladugu, J. Zou, J.N. Guo, X. Zhang, Y. Kim, H.J. Joyce, Q. Gao, H.H. Tan, C. Jagadish, Nature of heterointerfaces in GaAs/InAs and InAs/GaAs axial nanowire heterostructures, Appl. Phys. Lett., 93 (2008) 101911-101914.

[4] M.E. Messing, J. Wong-Leung, Z. Zanolli, H.J. Joyce, H.H. Tan, Q. Gao, L.R. Wallenberg, J. Johansson, C. Jagadish, Growth of Straight InAs-on-GaAs Nanowire Heterostructures, Nano Lett., 11 (2011) 3899-3905.

[5] K.A. Dick, J. Bolinsson, B.M. Borg, J. Johansson, Controlling the Abruptness of Axial Heterojunctions in III–V Nanowires: Beyond the Reservoir Effect, Nano Lett., 12 (2012) 3200-3206.

[6] A.N. Torgersen, L. Offernes, A. Kjekshus, A. Olsen, The tin-rich part of the Au–Pt–Sn system, J. Alloys Compd., 314 (2001) 92-95.

[7] K. Schubert, H. Breimer, R. Gohle, H.L. Lukas, H.G. Meissner, E. Stolz, Einige strukturelle Ergebnisse an metallischen Phasen III, Naturwissenschaften, 45 (1958) 360-361.

[8] V. Petricek, M. Dusek, L. Palatinus, Jana2006. The crystallographic computing system, in, Institute of Physics, Praha, Czech Republic, , 2006.

[9] L. Palatinus, G. Chapuis, SUPERFLIP - a computer program for the solution of crystal structures by charge flipping in arbitrary dimensions, J. Appl. Crystallogr., 40 (2007) 786-790.

[10] O.K. Andersen, The Stuttgart Tight-Binding LMTO-ASA program Version 4.7, in, Max-Planck-Institut für Festkörperforschung Germany, 2000.

[11] U. von Barth, L. Hedin, A local exchange-correlation potential for the spin polarized case. i, J. Phys. C: Solid State Physics, 5 (1972) 1629-1642.

[12] R. Dronskowski, P.E. Bloechl, Crystal orbital Hamilton populations (COHP): energy-resolved visualization of chemical bonding in solids based on density-functional calculations, The Journal of Physical Chemistry, 97 (1993) 8617-8624.

[13] X. Gonze, J.M. Beuken, R. Caracas, F. Detraux, M. Fuchs, G.M. Rignanese, L. Sindic, M. Verstraete, G. Zerah, F. Jollet, M. Torrent, A. Roy, M. Mikami, P. Ghosez, J.Y. Raty, D.C. Allan, First-principles computation of material properties: the ABINIT software project, Comput. Mater. Sci., 25 (2002) 478-492.

[14] X. Gonze, A brief introduction to the ABINIT software package, Zeitschrift für Kristallographie, 220 (2005) 558-562.

[15] X. Gonze, B. Amadon, P.M. Anglade, J.M. Beuken, F. Bottin, P. Boulanger, F. Bruneval, D. Caliste, R. Caracas, M. Côté, T. Deutsch, L. Genovese, P. Ghosez, M. Giantomassi, S. Goedecker, D.R. Hamann, P. Hermet, F. Jollet, G. Jomard, S. Leroux, M. Mancini, S. Mazevet, M.J.T. Oliveira, G. Onida, Y. Pouillon, T. Rangel, G.M. Rignanese, D. Sangalli, R. Shaltaf, M. Torrent, M.J. Verstraete, G. Zerah, J.W. Zwanziger, ABINIT: First-principles approach to material and nanosystem properties, Comput. Phys. Commun., 180 (2009) 2582-2615.

[16] J.P. Perdew, K. Burke, M. Ernzerhof, Generalized Gradient Approximation Made Simple, Phys. Rev. Lett., 77 (1996) 3865-3868.

[17] M. Fuchs, M. Scheffler, Ab initio pseudopotentials for electronic structure calculations of poly-atomic systems using density-functional theory, Comput. Phys. Commun., 119 (1999) 67-98.

[18] H.J. Monkhorst, J.D. Pack, Special points for Brillouin-zone integrations, Phys. Rev. B, 13 (1976) 5188-5192.

[19] M. Methfessel, A.T. Paxton, High-precision sampling for Brillouin-zone integration in metals, Phys. Rev. B, 40 (1989) 3616-3621.

[20] M. Ghasemi, S. Lidin, J. Johansson, The phase equilibria in the Au-In-Ga ternary system, Submitted.

[21] K. Schubert, H. Pfisterer, Kristallstruktur von Pt_2Sn_3, Z. Metallkd, 40 (1949) 405-411.

[22] B.Y. Tsaur, J.W. Mayer, K.N. Tu, Ion-beam induced metastable Pt_2Si_3 phase. I. Formation, structure, and properties, J. Appl. Phys., 51 (1980) 5326-5333.

Table 1. The results of crystal structure refinement.

Crystal data		***Data collection***	
Au_2InGa_2	D_x = 10.797 Mg m^{-3}	Agilent technologies EOS diffractometer	R_{int} = 0.190
M_r = 648.2	Melting point: 667 K	Radiation source: X-ray tube	θ_{max} = 28.0°, θ_{min} = 3.1°
Hexagonal, $P6_3/mmc$	Mo $K\alpha$ radiation,		
	λ = 0.71069 Å		-5 ≤ h ≤ 4
Hall symbol: -P 6c;-2c			-2 ≤ k ≤ 5
a = 4.2099 (4) Å[1]		1438 measured reflections	-16 ≤ l ≤ 16
c = 12.9863 (12) Å[1]	μ = 92.14 mm^{-1}	121 independent reflections	
V = 199.32 (3) Å^3	T = 293 K	97 reflections with $I > 3\sigma(I)$	
Z = 2	Irregular shape		
F(000) = 538	0.1×0.1 ×0.1 mm		

Refinement

Refinement on F^2	Primary atom site location: Superflip
$R[F^2 > 2\sigma(F^2)]$ = 0.036	Weighting scheme based on measured s.u.'s $w = 1/(\sigma^2(I) + 0.0016I^2)$
$wR(F^2)$ = 0.084	$(\Delta/\sigma)_{max}$ = 0.019
S = 1.43	$\Delta\rho_{max}$ = 2.75 e Å^{-3}
121 reflections	$\Delta\rho_{min}$ = −2.81 e Å^{-3}
10 parameters	Extinction correction: B-C type 1 Gaussian isotropic (Becker & Coppens, 1974)
0 restraints	Extinction coefficient: 36 (13)
0 constraints	

Fractional atomic coordinates and isotropic or equivalent isotropic displacement parameters (Å^2)

	x	y	z	U_{iso}*/U_{eq}
Au1	1/3	2/3	0.13931 (11)	0.0141 (4)
In1	0	0	0.25	0.0148 (9)
Ga1	1/3	2/3	0.5633 (3)	0.0126 (9)

Atomic displacement parameters (Å^2)

	U^{11}	U^{22}	U^{33}	U^{12}	U^{13}	U^{23}
Au1	0.0139 (5)	0.0139 (5)	0.0146 (8)	0.0069 (3)	0	0
In1	0.0112 (9)	0.0112 (9)	0.0219 (19)	0.0056 (4)	0	0
Ga1	0.0109 (10)	0.0109 (10)	0.016 (2)	0.0055 (5)	0	0

Bond lengths (Å)

Au1—Au1^{i}	2.875 (2)	Au1—Ga1^{v}	2.6232 (18)
Au1—In1^{ii}	2.8238 (9)	Au1—Ga1^{vi}	2.632 (4)
Au1—In1	2.8238 (8)	Ga1—Ga1^{vii}	2.935 (3)
Au1—In1^{iii}	2.8238 (9)	Ga1—Ga1^{vi}	2.935 (3)
Au1—Ga1^{iv}	2.6232 (18)	Ga1—Ga1^{viii}	2.935 (3)
Au1—Ga1	2.6232 (17)		

Symmetry codes: (i) −y+1, −x+1, −z+1/2; (ii) x, y−1, z; (iii) x+1, y, z; (iv) x−1, y, z; (v) x, y+1, z; (vi) y, x, −z; (vii) y, x−1, −z; (viii) y+1, x, −z.

Table 2. The negative integrated -ICOHP values at the Fermi level.

Bonds	Distance (Å)	Number per Cell	-ICOHP(E_F) per Bond (eV)	-ICOHP(E_F) per Cell (eV)
Au-Ga	2.623	× 12	1.78	21.38
	2.631	× 4	1.64	6.55
Au-In	2.824	× 12	1.32	15.79
Au-Au	2.875	× 2	1.07	2.14
Ga-Ga	2.934	× 6	0.65	3.93
Ga-In	3.433	× 12	0.22	2.64

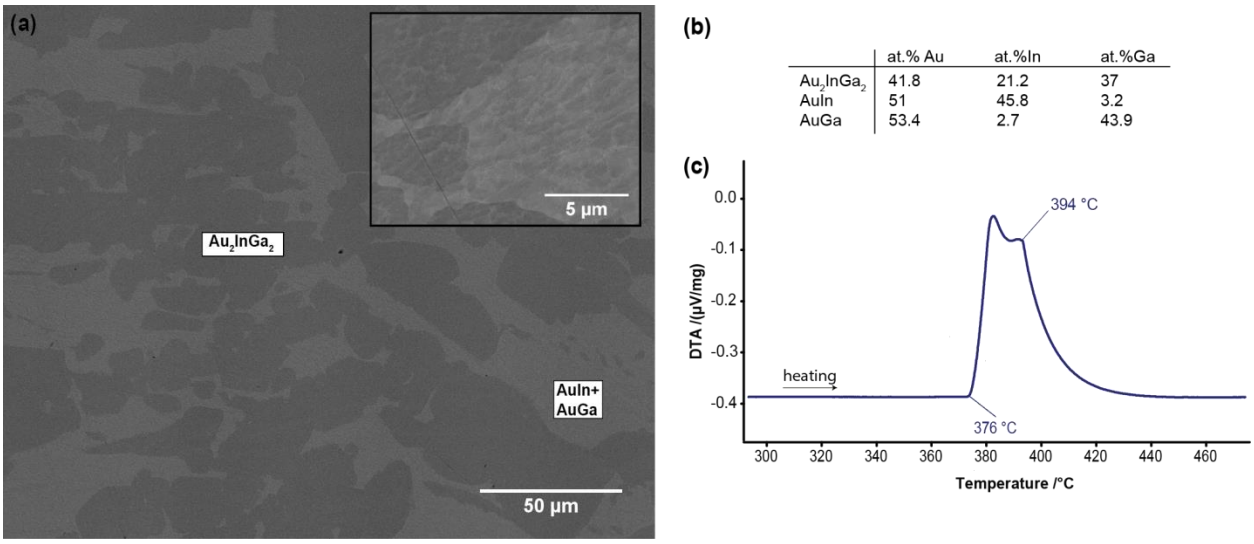

Figure 1. (a) Post-DTA microstructures of the sample with the composition of 44 at.% Au-22 at.% In-34 at.% Ga. The magnified view is shown in the inset. The micrographs show a three-phase field region: Au_2InGa_2, AuIn and AuGa. There is significant solubility of Ga in AuIn and of In in AuGa (the region in light gray). (b) EDS spectra of the coexisting phases. The elemental compositions are the average value of the compositions on different spectra. (c) DTA thermogram of the same sample recorded with the rate of 10 °C/min.

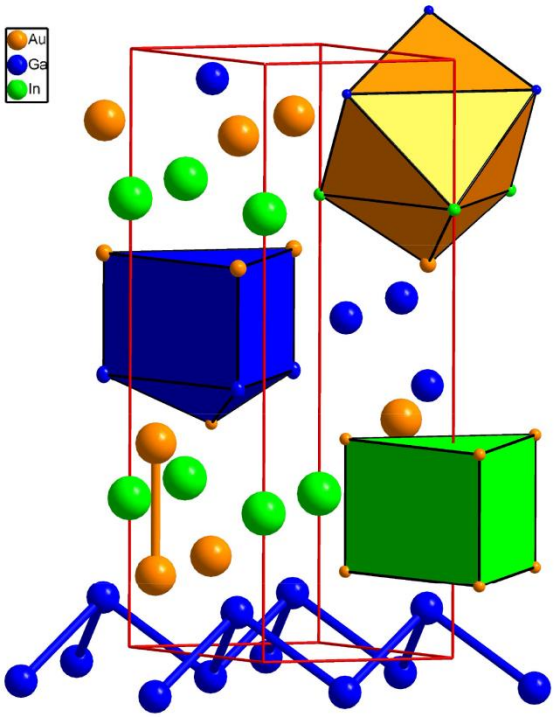

Figure 2. Structure of Au_2InGa_2. Indium is shown in green, gallium in blue and gold in gold. The coordination polyhedral of each species is shown colored by the code of the central atom, and in the lower part of the unit cell, the patterns of short, homoatomic distances, a puckered 6^3 net for gallium and dumbbells for gold, is highlighted.

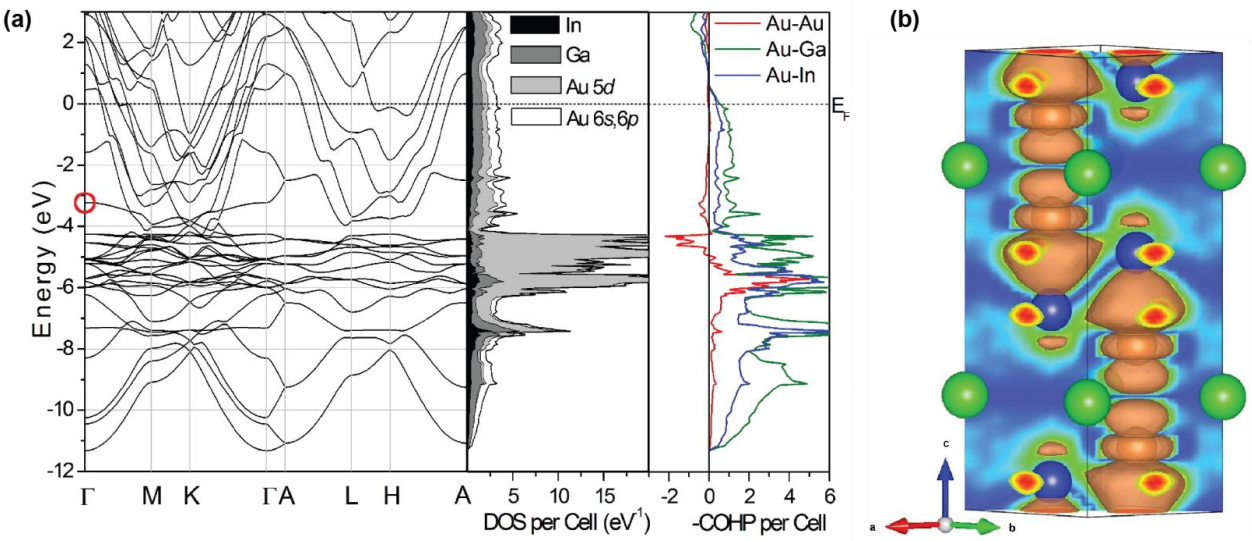

Figure 3. (a) The band structure, DOS, and -COHP curves of Au_2InGa_2 calculated with LMTO. (b) The wavefunction norm plot of the second highest occupied band at the Γ point. Loci of atoms are indicated with spheres, gold for Au, green for In and blue for Ga.

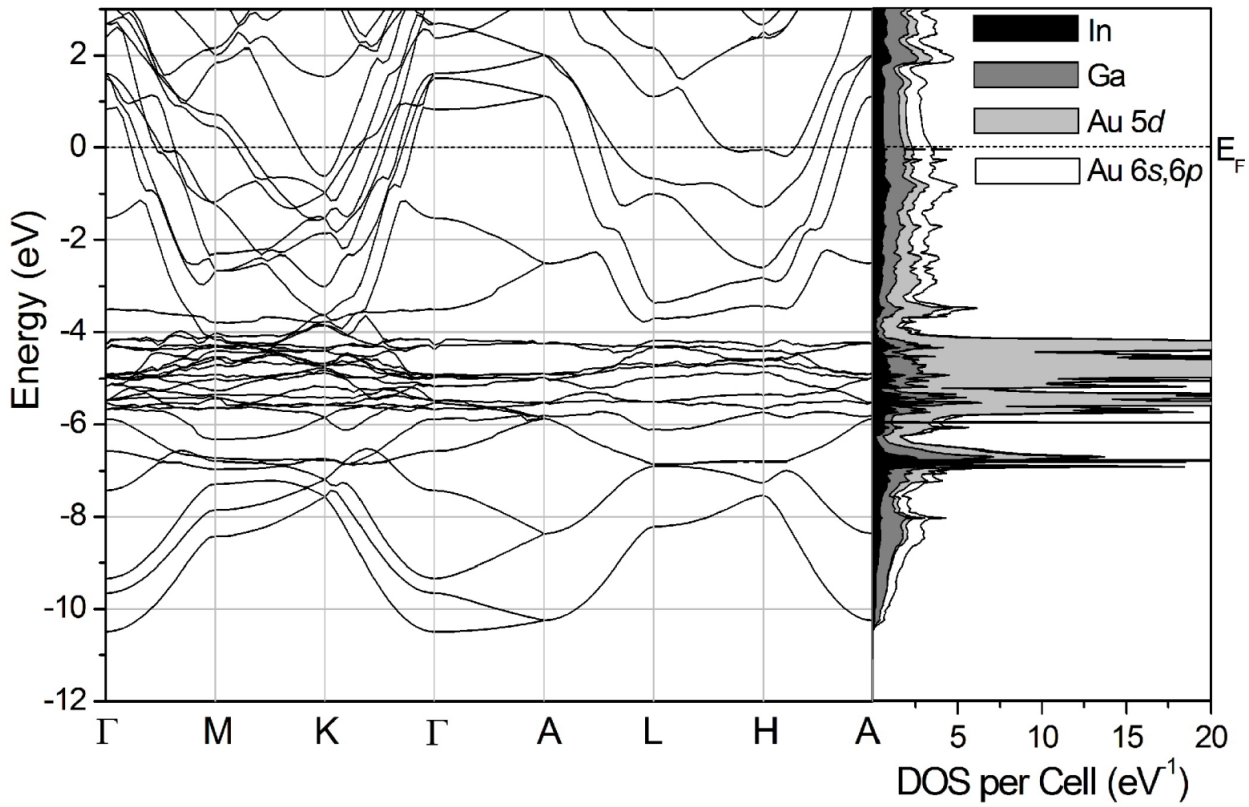

Figure S1. The band structure and DOS curves calculated with ABINIT.